LA-UR-01-4473
Approved for public release;
distribution is unlimited.

Title: A 75-keV, 140-mA Proton Injector

Author(s): Joseph D. Sherman, Terry L. Figueroa, Lash D. Hansborough, Debora M. Kerstiens, J. David Schneider, H. Vernon Smith, Jr., Matthew W. Stettler, Ralph R. Stevens, Jr., Michael E. Thuot, David S. Warren, Thomas J. Zaugg, Adrian A. Arvin, Alvin S. Bolt and Jack E. Boers

Submitted to:

http://lib-www.lanl.gov/la-pubs/00796317.pdf

A 75-keV, 140-mA Proton Injector

Joseph D. Sherman, Terry L. Figueroa, Lash D. Hansborough, Debora M. Kerstiens, J. David Schneider, H. Vernon Smith, Jr., Matthew W. Stettler, Ralph R. Stevens, Jr., Michael E. Thuot, David S. Warren, Thomas J. Zaugg
Los Alamos National Laboratory, Los Alamos, New Mexico 87545

Adrian A. Arvin and Alvin S. Bolt
Savannah River Site, Aiken, South Carolina 29841

Jack E. Boers, Thunderbird Simulations, Garland, Texas75042

A dc and pulsed-mode 75-keV proton injector has been developed and is used in characterization of a continuous-wave (cw) 6.7-MeV, 100-mA radio-frequency quadrupole (RFQ). The injector is used frequently at the full RFQ design power (100-mA, 6.7-MeV) where the RFQ admittance (1rms, normalized) is 0.23 (πmm-mrad). The injector includes a 2.45-GHz microwave proton source and a beam space-charge-neutralized, two magnetic-solenoid, low-energy beam-transport system (LEBT). The design RFQ beam transmission of 95% has been demonstrated at 100-mA RFQ output current.

I. Introduction

The injector uses a microwave (2.45 GHz) proton source[1] and a two-solenoid low-energy beam transport system[2] (LEBT) to match proton beams into a 6.7-MeV radio frequency quadrupole (RFQ).[3] The design and operation of a 75-keV, 130-mA proton injector has been previously described.[4] The injector was previously configured to operate at 50-keV energy for injection into a 1.25-MeV cw radio-frequency quadrupole (RFQ).[5] The 50-keV injector did provide proton beams that allowed the 1.25-MeV RFQ to exceed its original output design current.[6] The proton injector has now been configured for the 75-keV operation, leading to the demonstration of a 100-mA cw and pulsed mode beams from a 6.7-MeV RFQ.[7] Section II summarizes the 75-keV injector development while section III presents the results of using the injector on the 6.7-MeV RFQ. The multi-particle code PBGUNS[8] is used to analyze the beam propagation from the ion source plasma to the RFQ matchpoint.

II. Injector Development

Figure 1 shows a line drawing of the 75-keV proton source. The ion source plasma chamber and

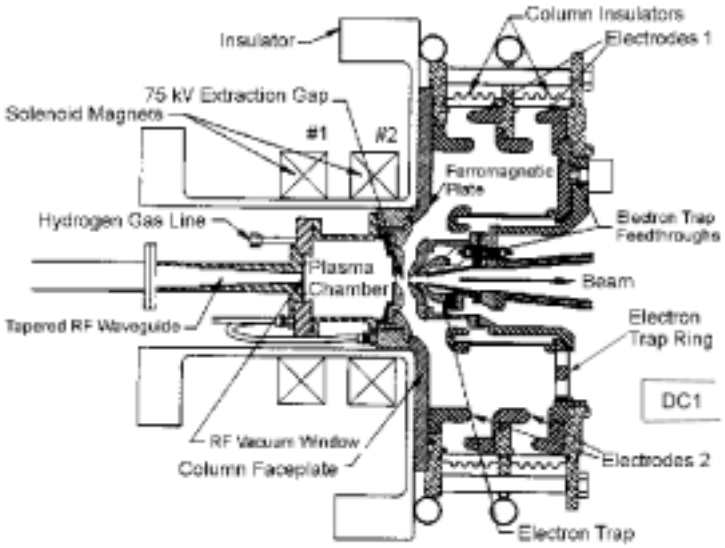

Figure 1. Line drawing for the 75-keV injector ion source.

a section of the 2.45-GHz waveguide operate at 75 kV-potential. These high-voltage components are separated from ground potential by the following: (1) a two segment ceramic (Al_2O_3) column which supports the beam formation electrodes, (2) a large-diameter polypropylene insulator which electrically insulates the ion source solenoid magnets from the 75-kV potential, (3) a high-voltage waveguide break (not shown) which electrically separates the 2.45-GHz magnetron tube from the 75-kV source, and (4) a small diameter H_2 insulated gas tube which allows the gas control system to operate at ground potential. This injector configuration avoids the use of a high-voltage isolation transformer, and lends itself to efficient high-voltage transient spark protection.[9]

Operating parameters for the microwave source are shown in Table 1. These parameters were retrieved from control-system[10] archived data of the 6.7-MeV RFQ operation on Feb. 14, 2000. The

Table 1. Summary of the proton source operation.

Ion Source Parameter	Value
H_2 gas flow, Q_{H2} (sccm)	4.1
Ion source pressure (mTorr)	2
Ion source gas efficiency (%)	24
Discharge power, 2.45 GHz (kW)	1.2
Ion source solenoid 1 (A)	87.2
Ion source solenoid 2 (A)	89.2
Axial magnetic field, calculated (G)	863
Beam energy (keV)	75
High voltage power supply current (mA)	165
Electron trap voltage (kV)	-1.95
DC1 current (mA)	154
Beam current density (mA/cm^2)	265
Beam power, cw mode (kW)	11.6
Proton current at DC1 (mA)	139
Duty factor (%)	100
DC2 current (mA)	120
Injector emittance, 1rms norm. (πmm-mrad)	0.18

ion source pressure is calculated from the measured H_2 gas flow and the emission aperture radius r_{em} = 4.3mm assuming molecular flow through an aperture. The calculated 24% gas efficiency means that for 100 protons entering the plasma chamber in the form of H_2 gas, 24 emerge from the emission aperture as protons.[11] Earlier work on the microwave proton source indicated efficient operational modes with 875-G axial field (magnetic field for electron-cyclotron resonance at 2.45 GHz) near the microwave window.[4,12] A large amount of ion source solenoid data has been analyzed in a Quickfield magnetics model[13] for the 75-keV ion source configuration. The derived empirical relation for the solenoid B-field on axis at the microwave window location (cf Fig. 1) in the ion source is B_{window} (G)= 6.14*IS1 + 3.67*IS2 where IS1 and IS2 are the ion source solenoid currents in amperes. Applying this relation to the ion source solenoid data of Table 1, we find a value of 863G, close to the 875G resonant magnetic field. The ion source beam current density and beam power are calculated using the 154-mA DC1 current, r_{em}, and 75-keV beam energy. The proton current is calculated from the 154-mA beam current, and taking a proton fraction of 90%.[4] The measured injector emittance is 0.18(πmm-mrad) - see the discussion below for the injector beam emittance. Further ion source details can be found in ref. 4.

The extraction system geometry, temperature performance in cw mode, and electrode composition are summarized in Table 2. Moderate electrode temperatures (30-40 ^oC) are observed while in operation with perveance matched beams with the order of 12-kW beam power. Molybdenum is used for the extraction electrodes because of its non-magnetic, high melting temperature, and sputtering characteristics. Copper has performed well as the material for the plasma electrode. Figure 2 shows the beam formation electrodes, equipotentials, and trajectory plot obtained from the PBGUNS code[8] using the geometry contained in Table 2, with an injected current density of 265 mA/cm^2. This injected current density comes

from the ion source measurements contained in Table 1. The variable z is used to indicate the distance along the beam direction, and r is used for the transverse coordinate. This calculation gives 154-mA

Table 2. Tetrode ion extraction system.

Parameter	Dimension (mm)	Temperature (^{o}C)	Material
Plasma electrode radius (75 kV potential)	4.3	Not measured	Copper
Extraction gap	12.9		
Extraction electrode radius (First ground electrode)	3.3	42	Molybdenum
Electron suppressor electrode radius	4.4	40	Molybdenum
Electron suppressor electrode length	8.0		
Second ground electrode radius	4.5	28	Molybdenum

total current at the exit plane of the calculation (near z=54mm in Fig. 2), and agrees with the total measured current at DC1 (cf Table 1). An injected Maxwellian particle distribution corresponding to a 1.5-eV ion plasma temperature is used here. This ion temperature gives a predicted proton beam emittance (1rms, normalized) of 0.11(πmm-mrad) immediately after extraction, and agrees with earlier ion

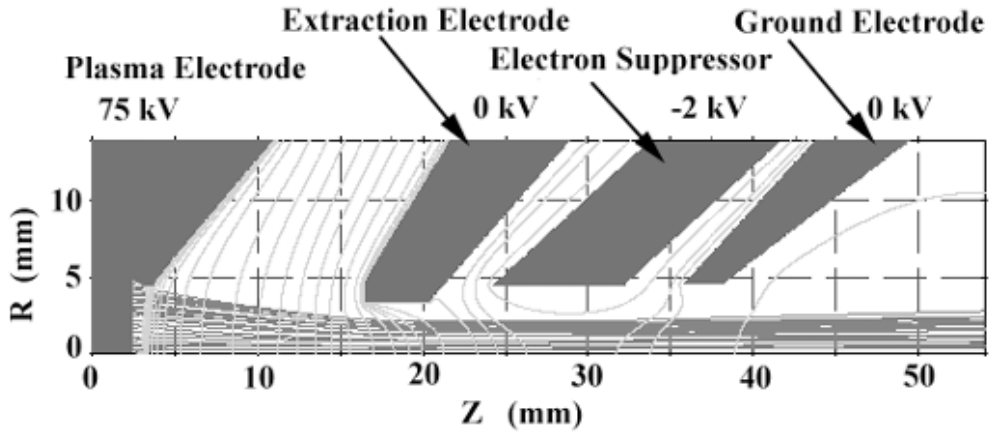

Figure 2. PBGUNS simulation for the 75-keV beam extraction electrodes. The calculation corresponds to the 154 mA total current accelerated through the DC1 beam current monitor with a 1.5 eV plasma ion temperature.

source-only beam emittance measurements.[14] Beam particle trajectories shown in the Fig. 2 plot are comprised of 90% protons and 10% H_2^+ ions at the beam energy of T_b = 75 keV. The electrode potentials relative to ground are shown. The electron suppressor electrode prevents electrons formed in the LEBT from back steaming to the ion source. The PBGUNS code uses the successive over-relaxation procedure to solve for the plasma emission surface (meniscus). The meniscus is the origin of the ion-optics modeled through the LEBT, and is discussed below.

Figure 3 shows the injector LEBT configuration as used in the 6.7-MeV RFQ experiments. The LEBT solenoid magnets S1 and S2 are used to capture the beam from the ion source, and then to focus the beam into the RFQ. Beam centroid control in the LEBT is accomplished by use of a pair of steering magnets SM1 and SM2 which move the beam in the transverse directions. The AC toroid monitors the injector beam noise,[4] and the beam stop allows high-power injector operation when no demand is made by the RFQ for beam. LEBT beam currents are monitored at the ion source exit (DC1), between the solenoid focus magnets (DC2), and at the RFQ entrance (after S2). There is a 5-cm diameter beam halo scraper located 10cm upstream from S1 entrance. A second beam collimator is located between

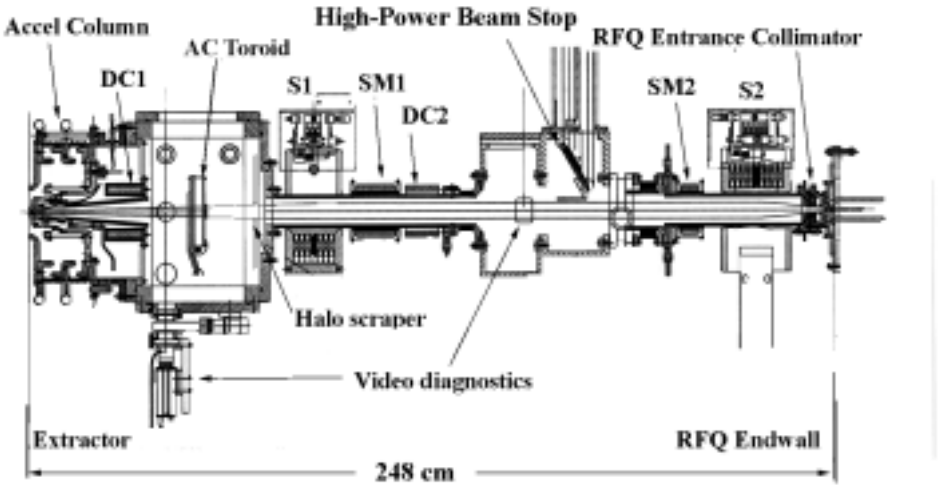

Figure 3. Line drawing for the 75-keV LEBT used in the 6.7-MeV RFQ experiments.

S2 and the RFQ entrance. This collimator prevents nearly all of the defocused H_2^+ beam from entering the RFQ. The exit of S2 is located 14cm from the RFQ entrance.

During the injector commissioning phase for 6.7-MeV RFQ operation, improved S1 pole faces were fabricated for RFQ beam matching. With the injector rolled back from the RFQ, and the cw emittance measurement unit in place,[4] 75-keV beam emittance measurements were made on the original pole faces (mod1), and then the improved pole faces (mod2). The results are shown in Fig. 4. Here the

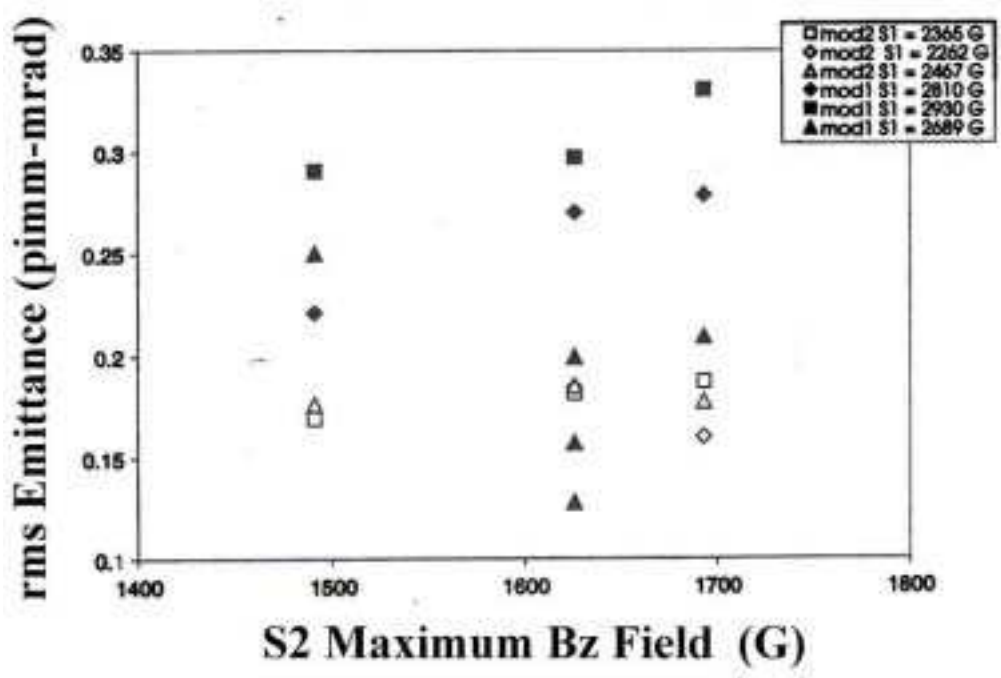

Figure 4. rms beam emittance measurements comparing the original (mod1) and improved (mod2) S1 pole faces. These emittances were obtained with the injector rolled back from the RFQ endwall.

measured rms normalized emittances are plotted vs the maximum on-axis field $(B_z)_{max}$ of S2. It was not possible to measure the beam emittance only through S1 as time restrictions did not allow installation of the emittance gear at the S1 exit. Further, it was not possible to operate S2 at current levels as for RFQ beam

matching condition because of the prohibitive beam power densities. Data are taken as a function of S1 excitation for the mod1 and mod2 pole faces. These excitations are shown as a function of B_z maximum noted in the Fig. 4 inset. The closed symbols correspond to mod1 and open symbols correspond to mod2 pole faces. The trend is clear – an improvement in the normalized rms beam emittance was achieved by modifying the S1 pole face. With the improved S1 pole faces, the injector emittance is now 0.18(πmm-mrad) (rms, normalized), as given in Table 1.

A detailed line drawing of the RFQ entrance collimator and beam current monitor is shown in Fig. 5. This assembly comprises three functions at the RFQ entrance: (1) traps LEBT electrons from approaching the RFQ and establishes a region of 100% beam space-charge decompensation; (2) provides a reliable differential current monitor so the beam entering the RFQ can be compared with the 6.7-MeV accelerated proton current; and (3) nearly eliminates the defocused H_2^+ beam. The beam-current measurement establishes the RFQ current transmission,[15] and is a fundamental measurement for confirmation of RFQ design.[7] The LEBT electron trap is operated at -1890V. Approximate dimensions for the RFQ entrance collimator are 7cm long by 1.7cm diameter. The RFQ entrance collimator was not installed during the emittance measurements discussed in Fig. 4.

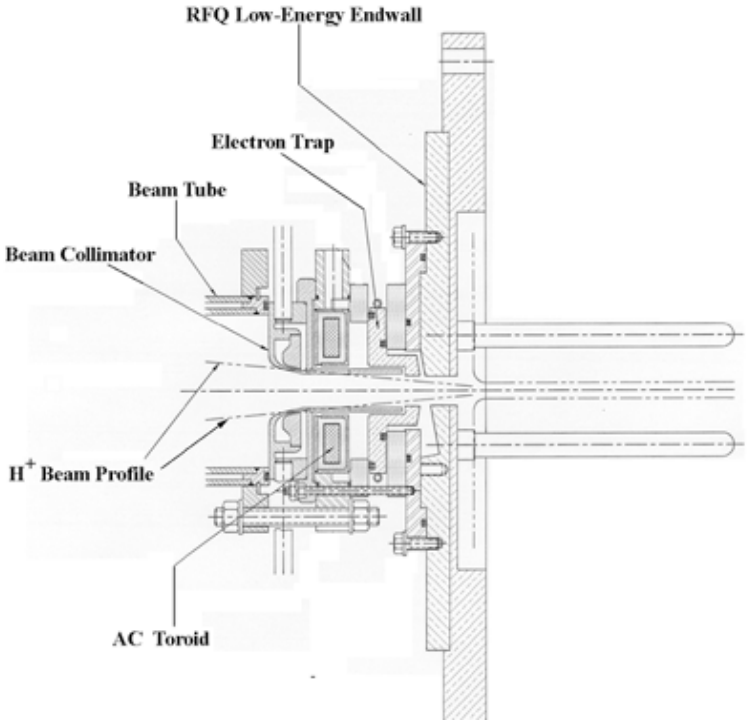

Figure 5. Entrance assembly to the 6.7 MeV RFQ.

Summary of the solenoid S1 and S2 design is contained in Table 3. The solenoid currents and the corresponding $(B_z)_{max}$ for injector operation at the RFQ output design current (100 mA) in cw mode are also contained in Table 3. These data are input to the injector model discussed in Section III.

Table 3. Summary of the LEBT solenoid design and injector operation during 100-mA cw mode RFQ operation.

Solenoid	Inside Diameter (cm)	Length (cm)	Number of Turns	Coil Current (A)	$(B_z)_{max}$ (G)
LEBT Solenoid 1 (S1)	10	17.5	126	299	3081
LEBT Solenoid 2 (S2)	10	21.6	168	369	4964

III. Discussion

For purpose of discussing the proton injector capabilities, we specifically discuss injector tuning for RFQ operation on the date of February 14, 2000 when the injector and RFQ were operated in cw mode. There is other literature discussion on the number of hours this facility has operated in cw mode,[16] and the 75-keV injector's availability and reliability while operating in stand-alone dc mode.[4] Figure 6 shows a contour plot of the 6.7-MeV RFQ transmission as a function of the S1 and S2 current settings. A rather narrow range of solenoid currents are attempted in tuning, as defocusing of the dc injector beam power at

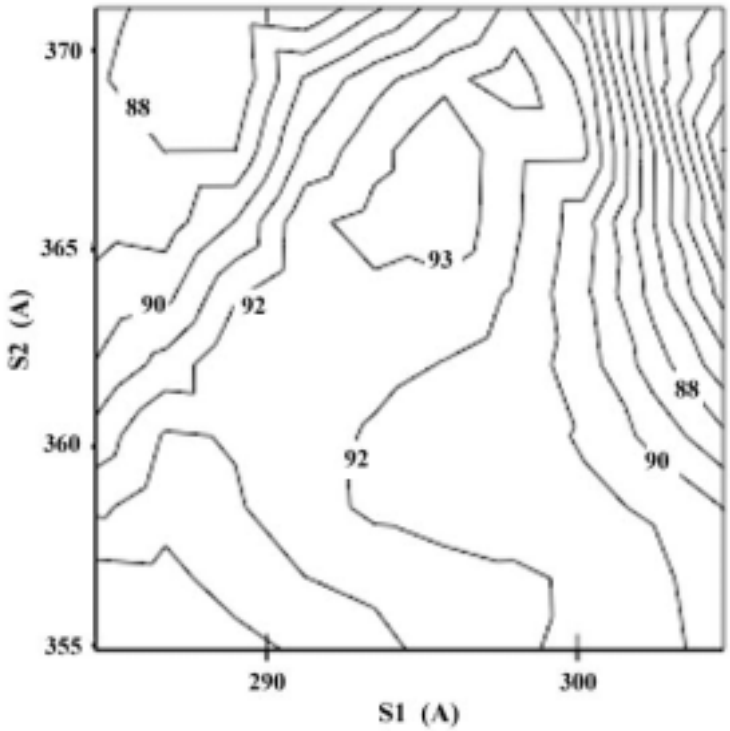

Figure 6. Measured transmission of the proton beam through the 6.7-MeV RFQ as a function of the LEBT solenoid currents S1 and S2. The highest transmission corresponds to current greater than 100 mA at 6.7 MeV.

this location, where the 75-keV beam power is approximately 9 kW, may damage the RFQ entrance collimator shown in Fig. 5. The peak transmission corresponds to greater than 100-mA current accelerated to 6.7 MeV.

The LEBT beam current data corresponding to the Fig. 6 RFQ transmission curves are 154 mA at DC1 and 120 mA at DC2 (cf Table 1). This corresponds to 140 and 108 mA proton currents at these two locations, assuming a 90% proton fraction. Considering a measured 94% RFQ transmission at 100-mA RFQ transmitted current, nearly all of the protons at the location of DC2 must be transmitted through the RFQ entrance collimator. At the halo scraper location (cf Fig. 3), it is thought the H^+ and H_2^+ beams lie on nearly the same trajectories because the beam ensemble has traversed only the residual ion source B-field in the extraction region. Thus the H^+ and H_2^+ currents are assumed to be equally attenuated by the halo scraper.

A multi-particle model based on the axisymmetric PBGUNS code[17] is now described. It models the beam from the ion source plasma to the RFQ matchpoint. The fixed parameters in this model are ion source extraction geometry as described in Table 2 and Fig. 2., LEBT solenoid design and excitation as per Table 3, and LEBT mechanical design as shown in Fig. 3. The LEBT mechanical design includes z-location and diameter of the halo scraper, RFQ entrance collimator discussed above, and the beam pipe

diameter of 8cm. The particle density injected into the PBGUNS plasma corresponds to 265mA/cm^2 (cf Table 1) with 90% H^+ and 10% H_2^+ positive ions. The modeled positive-ion current is divided up into approximately 2000 trajectories for most of the simulations. The degree of residual beam space-charge neutralization f is defined such that the effective current in beam transport is $I_{eff} = (1\text{-}f)I_b$, where I_b = measured beam current. The on-axis B_z field maps are taken from Vector Fields[18] axisymmetric models for the LEBT solenoids S1 and S2. These values are expanded off-axis according to standard approximations.[17,19] In order to fit the observed LEBT current losses and injector-RFQ beam match, the degree of beam space charge compensation in the LEBT is allowed freedom to vary. Recent work on a similar proton injector[20] has indicated f may be lower than that used in previous LEBT modeling.[5,21] The ion source temperature kT_i = 1.5eV is determined by fitting measured beam emittance for ion-source only measurements (see discussion above). This model is similar to that reported for the 50-keV injector used on the 1.25-MeV cw RFQ.[5]

Fig. 7 summarizes the PBGUNS trajectory calculations with the attendant ion source extraction electrodes, beam collimators, beam pipes, electron traps, and LEBT solenoid magnets. The PBGUNS plots show the z locations of the injector components relative to a z=0 near the ion source plasma. Note that the LEBT z coordinate in Fig. 3 starts at the front surface of the extraction electrode, thus a correction of −1.6cm needs to be applied to the PBGUNS z coordinate when comparing with the LEBT mechanical engineering diagram shown in Fig. 3.

Fig. 7(A) shows the ion source plasma, beam extraction system, and a long drift (20cm) which allows the beam to grow radially to 10mm radius before entering the first LEBT segment. To maintain sufficient numerical accuracy, the voltage and space-charge simulation matrices are defined to be 2501 (z) by 141 (r) matrix units with 0.1mm/matrix square. Other than the additional length, the ion source model is identical to that shown in Fig. 2. The full beam space charge is effective (f=0) in the ion source z location from the plasma meniscus to approximately z=4cm, where compensation of the beam space-charge becomes effective by the trapping of beam plasma electrons within the positive-ion beam potential and the axial electron trap potential. In the ion source drift section from 4cm to 24cm, f=0.945. The next section of the simulation shown in Fig. 7(B) contains the halo scraper located at z=74cm, and the solenoid S1 located at z=90cm. Because the beam has grown radially to 10mm, the matrix size in the LEBT segments is increased to 1mm/matrix square. The LEBT segment S1 is thus calculated based on matrix sizes 1341 (z) by 51 (r). The B_z normalized profile is shown in the upper portion of Fig. 7(B), where the $(B_z)_{max}$ = 3081G (see Table 3). The (r,r') particle coordinates calculated in segment 7(A) are used as starting values in the LEBT segment S1. This trajectory restart procedure is also used in the following two simulation sections. By taking f = 0.945 for the ion source drift region and f = 0.94 in LEBT segment S1, 34 mA beam is simulated to be lost at the halo scraper, and the DC2 current of 120 mA is reproduced. The simulated proton emittance after S1 is 0.17(πmm-mrad), in good agreement with the measured results shown in Fig. 4.

LEBT segment S2 simulation includes solenoid S2 located at z=225cm and the first section of the RFQ entrance collimator located at z=240cm. Figure 7(C) shows the S2 normalized axial B-field B_z at r=0 where $(B_z)_{max}$ = 4964G (see Table 3), and the calculated trajectories in LEBT segment S2 below. With an f = 0.94, all of the proton beam from the halo scraper is focused through the RFQ entrance collimator aperture, giving a predicted 108-mA proton current at the RFQ entrance. The LEBT segment S2 is contained within PBGUNS matrix sizes of 911 (z) by 51 (r) with 1mm/matrix square length. The simulated injector proton emittance at the end of LEBT segment S2 is 0.19(πmm-mrad). The final LEBT segment simulated in this model is the final part of the RFQ entrance collimator and the LEBT electron trap. This section is shown in Fig. 7(D). As in the high-electric field case on the ion source extraction region (Figs. 2 and 7(A)) the full beam space charge (f=0) is assumed to be present in the LEBT electron trap-RFQ entrance region. At the location z = 248.9cm, the simulated injector rms Courant-Snyder parameters are α_r = 1.949 and β_r = 0.1266 mm/mrad, quite close to the RFQ match condition. The emittance is predicted to

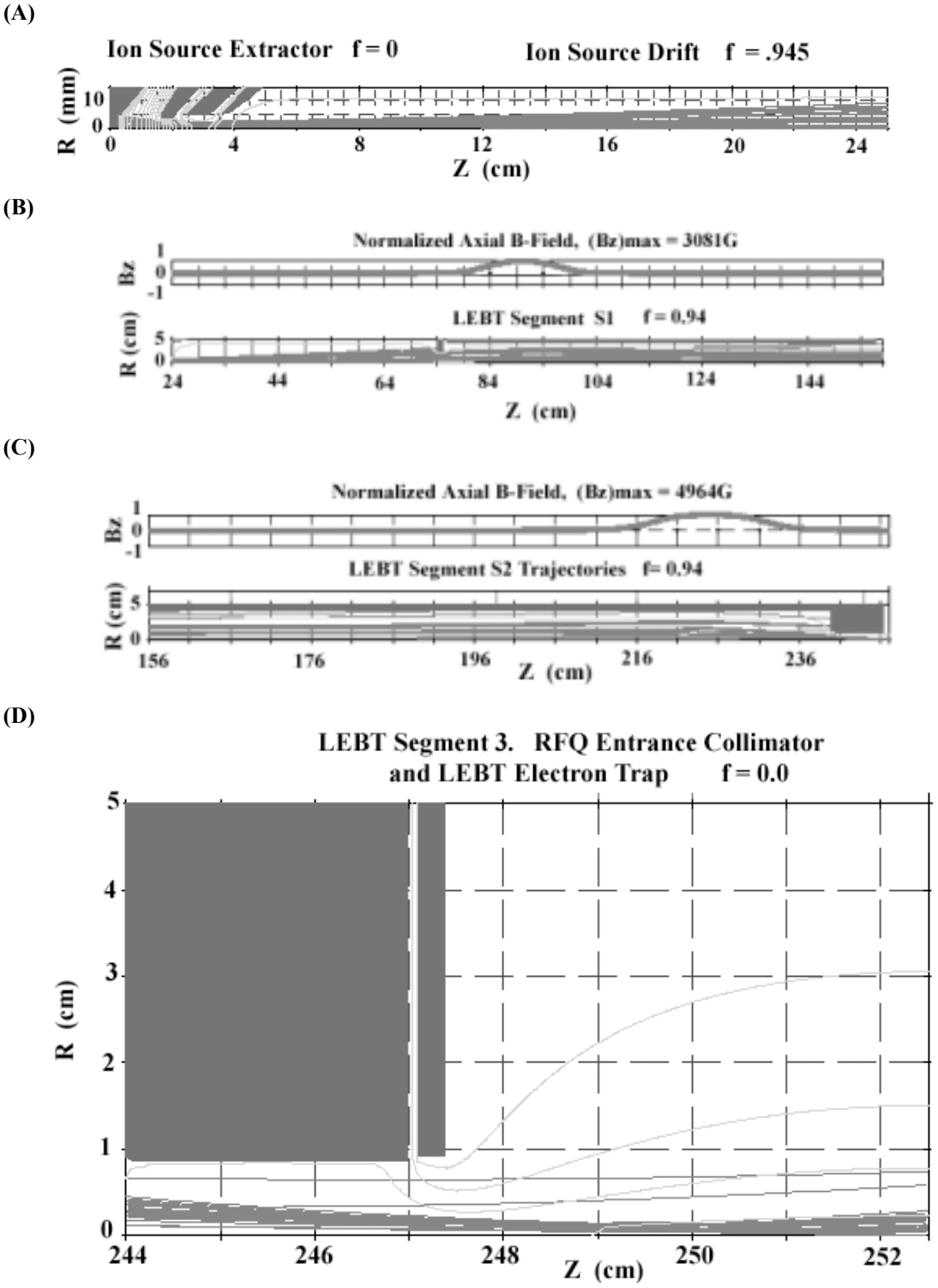

Figure 7. Shows the PBGUNS simulations for (A)the ion source and drift region, (B)the first LEBT segment S1, (C)the second LEBT segment S2, and (D)the final LEBT segment comprising the RFQ entrance collimator and LEBT electron trap.

decrease to 0.14(πmm-mrad) at this location. This simulated emittance decrease was checked by increasing the number of trajectories from 2000 to 5000, and changing the matrix size for the Fig. 7(D) simulation. In each of these cases the simulated emittance decrease was observed. The matrix sizes for the Fig. 7(D) simulation is 860 (z) by 501 (r) where the scale of 0.1mm/matrix square is used as in Fig. 7(A). The finer position step is used to better simulate the decreasing beam size as the beam approaches the RFQ matchpoint.

The simulation in Fig. 7(C) at the exit of S2 shows that the beam would be over-focused (Courant-Snyder α parameter too large), but application of the full beam space charge in the simulation of Fig. 7(D) causes sufficient beam defocusing to give the desired RFQ match. The z location of the simulated matched beam parameters in the PBGUNS coordinates (248.9cm), gives a reasonable agreement of the overall injector length of 248cm from the extractor to the RFQ endwall shown in Fig. 3. The H_2^+ current predicted to pass through the RFQ entrance collimator is 0.4 mA. Very few of these H_2^+ ions are predicted to have a transverse phase-space falling within the RFQ acceptance (see following discussion).

Figure 8 shows a plot of the PBGUNS simulated H^+ and H_2^+ (r,r') phase space at z = 248.9 cm. For comparison, a semi-ellipse corresponding to the nominal 6.7-MeV RFQ admittance phase-space is shown. This ellipse is calculated based on the RFQ design Courant-Snyder parameters of α = 1.944 and

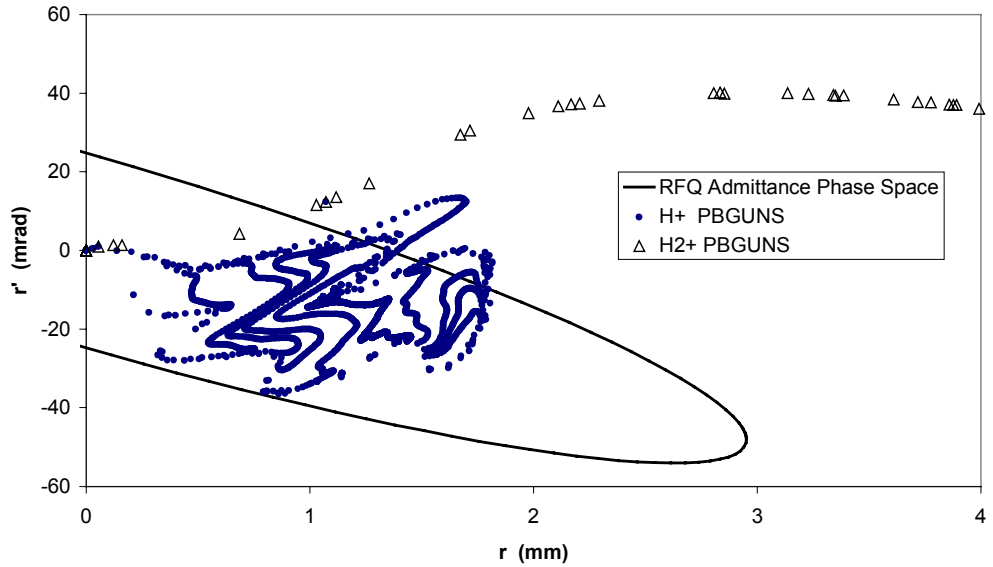

Figure 8. Comparison of the PBGUNS simulation for the H^+ and H_2^+ ion distributions near the 6.7-MeV RFQ matchpoint. The nominal RFQ phase-space admittance ellipse is shown for comparison.

β = 0.1193 (mm/mrad), and the laboratory phase-space area (emittance) of 73(πmm-mrad). The rms Courant-Snyder parameters calculated from the PBGUNS proton distribution shown in Fig. 8 are α_r = 1.949 and β_r = 0.1266 mm/mrad. The radial matching section[22] of the RFQ transforms the time independent injector (r,r') distribution to time dependent distributions in the transverse (x,x') and (y,y') planes. In Fig. 8, the limit of $\alpha_r = \alpha_x$ and $\beta_r = \beta_x$ is shown for the orientation of RFQ admittance phase-space.[23] A detailed RFQ simulation[7] is required to determine the RFQ efficiency in capturing the proton (r,r') trajectories shown in Fig. 8. A few of the H_2^+ ion trajectories fall within the RFQ acceptance, but most of the H_2^+ trajectories fall outside the RFQ acceptance ellipse.

Some discussion of the injector beam simulation as regards injector measurements should be made. The f = 0.945 in the ion source drift region (Fig. 7(A)) seems low. Earlier beam space-charge

neutralization measurements on this 75-keV injector[24] and measurements on a similar 95-keV injector[20] would suggest f = 0.97 to 0.98 would be more appropriate. Use of more effective beam current in the drift region from the ion source to the halo scraper may be masking an undetected beam steering effect. Such a steering effect would cause more beam attenuation at the halo scraper, thus increasing f towards closer agreement with the measurements. Examination of Fig. 8 in the r = 0 to 0.4mm region shows a hollowing of the beam at the RFQ match point. It is an open question whether this is a real physical effect or an artifact of handling on-axis beam charge for a long problem using an axisymmetric code. The z location of the matched beam as simulated by PBGUNS is near but not exactly on the mechanical design, and it is a more difficult task to model and measure this location precisely. However, the injector described here has enough tuning flexibility that trained operators can match the injector beam into the RFQ reproducibly.

This proton injector concept has now been successfully demonstrated on two cw RFQs. The first RFQ (1.25-MeV output energy) required 122-mA beam current at 50-keV energy,[5] and the first operation of this 6.7-MeV RFQ required 154-mA current at 75 keV. The 50-keV beam corresponds to a proton perveance $P = (m_p/m_e)^{1/2}(I(A)/(T_b(eV))^{3/2}$ of 0.47 micropervs while the 75-keV beam's perveance on the same perveance scale is 0.32 micropervs. One may use such a scale to compare feasibilities of various injector designs as applied to RFQ operations.

Acknowledgements

This work was supported by US DOE, NNSA and the Office of Nuclear Energy, Science and Technology. Joseph Sherman would like to acknowledge the support of CEA (Saclay, France) for support during preparation of this paper.

References

[1]T. Taylor and J. F. Mouris, Nucl. Instrum. Methods Phys. Res. A **336**, 1(1993).
[2]Ralph R. Stevens, Jr., AIP Conf. Proc. **287**, 646 (1992).
[3]D. Schrage, L. Young, P. Roybal, A. Naranjo, D. Baca, W. Clark, F. Martinez, H. Haagenstad, J. Mitchell, D. Montoya, A. Rendon, F. Krawczyk, T. Davis, D. Casillas, A. Gonzales, G. Gonzales, S. Hidalgo, E. Kettering, G. Leeches, B. Ormond, R. Reinert, O. Smith, and J. Tafoya, Linac Proceedings of the XIX International Linac Conference, Chicago, Illinois, Argonne National Laboratories Report, ANL-98/28, p. 679 (1998).
[4]Joseph Sherman, Andrew Arvin, Lash Hansborough, David Hodgkins, Earl Meyer, J. David Schneider, H. Vernon Smith, Jr., Matthew Stettler, Ralph R. Stevens, Jr., Michael Thuot, and Thomas Zaugg, Rev. Sci. Instrum. **69**, 1003 (1998).
[5]Joseph D. Sherman, Gerald O. Bolme, Lash D. Hansborough, Thomas W. Hardek, Debora M. Kerstiens, Earl A. Meyer, J. David Schneider, H. Vernon Smith, Jr., Matthew W. Stettler, Ralph R. Stevens, Jr., Michael E. Thuot, Thomas Zaugg, Adrian A. Arvin, Alvin S. Bolt, Patrick H. Hegler, Mitchell C. Richards, Jack E. Boers, James H. Kamperschroer, and Terry L. Figueroa, Rev. Sci. Instrum. **71**, 767 (2000).
[6]B. G. Chidley, F. P Adams, G. E. McMichael, T. Tran Ngoc, and T. S. Bhatia, Proceedings of the 1990 Linear Accelerator Conference, Los Alamos Report No. LA-12004-C, p. 42 (1991).
[7]L. M. Young, L. J. Rybarcyk, J. D, Schneider, M. E. Schulze, and H. V. Smith, Proceedings of the XX International Linac Conference, Stanford Linear Accelerator Report, SLAC-R-561, p. 336(2000).
[8]J. E. Boers, Proceedings of the 1995 Particle Accelerator Conference, IEEE Catalog No. 95CH35843, p. 2312.
[9]M. Thuot, L. R. Dalesio, M. Harrington, D. Hodgkins, D. Kerstiens, B. Quintana, J. D. Sherman, M. Stettler, D. Warren, T. Zaugg, A. Arvin, S. Bolt, and M. Richards, Proceedings of the 1999 Particle Accelerator Conference, IEEE Catalog No. 99CH36366, p. 349.
[10]L. Dalesio, D. Kerstiens, P. McGehee, M. Pieck, M. Stettler, R. Wright, D. Moore, D. Floersch, Proceedings of the 1999 Particle Accelerator Conference, IEEE Catalog No. 99CH36366, p. 652.
[11]Ralph R. Stevens, Jr., Joseph D. Sherman, and J. David Schneider, Proceedings of the 1993 Particle Accelerator Conference, IEEE Catalog No. 93CH3279-7, p. 3166.

[12]J.-M. Lagniel, P.-Y. Beauvais, D. Bogard, G. Bourdelle, G. Charruau, O. Delferriere, D. De Menezes, A. France, R. Ferdinand, Y. Gauthier, R. Gobin, F. Harrault, J.-L. Jannin, P.-A. Leroy, I. Yao, P. Ausset, B. Pottin, N. Rouviere, L. Celona, and S. Gammino, Rev. Sci. Instrum. **71**, 830 (2000).
[13]TERA Analysis Ltd., Knasterhovvej 21, DK-5700, Svenborg, Denmark.
[14]Terence Taylor and John S. C. Wills, Nucl. Instrum. Methods A **309**, 37 (1991).
[15]J. D. Gilpatrick, D. Barr, J. Power, W. C. Sellyey, R. Shurter, M. Stettler, J. Kamperschroer, D. Martinez, and J. O'Hara, Proceedings of the 1999 Particle Accelerator Conference, IEEE Catalog No. 99CH36366, p. 2214.
[16]H. Vernon Smith, Jr., and J. D. Schneider, Proceedings of the XX International Linac Conference, Stanford Linear Accelerator Report, SLAC-R-561, p. 581 (2000).
[17] Jack Boers, PBGUNS Users Manual, Thunderbird Simulations, Garland, Texas75042-6005.
[18]Vector Fields Ltd., 24 Bankside, Kidlington, Oxford OX5 1JE, England.
[19]Martin Reiser, Theory and Design of Charged Particle Beams, John Wiley and Sons, p. 66. (1994).
[20]P-Y. Beauvais, R. Ferdinand, R. Gobin, J. M. Lagniel, P-A. Leroy, L. Celona, G. Ciavola, S. Gammino, B. Pottin, and J. Sherman, Rev. Sci. Instrum. **71**, 1413 (2000).
[21]Lloyd M. Young, Proceedings of the 1997 Particle Accelerator Conference, IEEE Catalog No. 97CH36167, p. 2749.
[22]K. R. Crandall, Proceedings of the 1984 Linear Accelerator Conference, GSI Report, GSI-84-11, p. 581 (1984).
[23]Nicolas Pichoff, CEA (Saclay, France), unpublished notes.
[24]R. Ferdinand, J. Sherman, R. R. Stevens, Jr., and T. Zaugg, Proceedings of the 1997 Particle Accelerator Conference, IEEE Catalog No. 97CB36167, p. 2723.